Journal of Power Sources 201 (2012) 66–71

Contents lists available at SciVerse ScienceDirect

Journal of Power Sources

journal homepage: www.elsevier.com/locate/jpowsour

Intermediate temperature solid oxide fuel cells with $Cu_{1.3}Mn_{1.7}O_4$ internal reforming layer

Chao Jin[a,b], Chenghao Yang[b], Honghe Zheng[a,*], Fanglin Chen[b,**]

[a] School of Energy, Soochow University, Suzhou 215006, PR China
[b] Department of Mechanical Engineering, University of South Carolina, Columbia, SC 29208, USA

ARTICLE INFO

Article history:
Received 10 September 2011
Received in revised form 24 October 2011
Accepted 31 October 2011
Available online 6 November 2011

Keywords:
Solid oxide fuel cell
Spinel catalyst
Methane
Carbon deposition

ABSTRACT

$Cu_{1.3}Mn_{1.7}O_4$ (CMO) spinel catalyst has been synthesized and characterized by X-ray diffraction (XRD), scanning electron microscopy (SEM) and temperature-programmed reduction (TPR) techniques. XRD and SEM results show that well dispersed fine Cu metallic particles were obtained after reduction by methane. TPR result shows that $Cu_{1.3}Mn_{1.7}O_4$–SDC has lower hydrogen consumption and exhibits better catalytic activity than the conventional Ni catalyst. As a result, $Cu_{1.3}Mn_{1.7}O_4$ spinel catalyst has been successfully developed as an internal reforming layer for Ni–SDC anode-supported solid oxide fuel cells (SOFCs) directly operating with methane as the fuel. The cell has demonstrated maximum power densities of 304 and 375 mW cm^{-2} at 650 and 700 °C, respectively, and has been successfully operated at a constant current load of 0.6 A cm^{-2} at 650 °C over 80 h using methane as the fuel and ambient air as the oxidant. No significant carbon deposition has been observed at selected regions of the Ni–SDC anode after the short-term operating of the cell using methane as the fuel. Using methane as the fuel, the cell with $Cu_{1.3}Mn_{1.7}O_4$ internal reforming layer exhibits similar reaction mechanism to that of H_2 oxidation on the Ni–YSZ anode.

1. Introduction

Solid oxide fuel cell (SOFC) is high temperature electrochemical device that converts chemical energy of a fuel directly into electrical energy and has been regarded as a promising energy conversion and generation system because of its low emission, high energy conversion efficiency and more adaptive fuel than either a conventional power plant or lower temperature polymer-based fuel cells [1–4]. Besides hydrogen fuel, hydrocarbons, alcohols, dimethyl ether and even solid carbon can all be utilized as potential fuels [5–7]. To date, nickel-based cermets are the most frequently used anode materials in the state-of-the-art SOFCs due to their high electrical conductivity and excellent activity for fuel oxidation. However, one significant technical barrier for the nickel-based anode is carbon deposition (coking) when exposing to practical hydrocarbon fuels, leading to rapid degradation of the cell performance.

For hydrocarbon-fueled SOFCs based on Ni cermets anode, two different strategies have typically been applied to suppress coke formation and maintain high cell power output. One is using external reforming technique to convert hydrocarbon fuels to syngas (H_2 + CO) before being introduced into the anode chamber [8], and the other is fabricating internal reforming layer on the surface of the anode [9–11]. The external reforming process not only adds equipments and treatment process which will reduce the overall SOFC energy conversion efficiency, but also produces additional greenhouse gases. Compared with external reforming strategy, the latter is to integrate the catalytic conversion of hydrocarbons to syngas with fuel cell electrochemical reaction internally, resulting in higher energy conversion efficiency [12]. Based on this strategy, direct-methane fueled SOFCs have been the subject of intensive research because natural gas (with methane as the main constituent) is an abundant and widely accessible fuel and methane is also the main component of biogas, a renewable energy resource.

In recent years, CuM_2O_4 (M = Fe, Al, etc.) spinel oxides have been extensively proposed as catalyts for methane reforming [13,14]. Compared with Ni-based catalysts with alumina or silica supports either in laboratory or at industrial-scale and conventional Cu–MO_x mixed catalyst, CuM_2O_4 spinel oxide exhibits excellent catalytic performance because a uniform dispersion of nano-sized Cu species could be obtained from the spinel structure. In our previous communication [11], we have demonstrated that a relatively stable direct methane SOFC could be obtained with high power output by applying $Cu_{1.3}Mn_{1.7}O_4$–SDC as the internal reforming layer. In this work, we have systematically evaluated the electrochemical performance of this type of direct methane-fueled SOFC with $Cu_{1.3}Mn_{1.7}O_4$ internal reforming layer.

* Corresponding author.
** Corresponding author. Tel.: +1 803 777 4875; fax: +1 803 777 0106.
E-mail addresses: hhzheng@suda.edu.cn (H. Zheng), chenfa@cec.sc.edu (F. Chen).

0378-7753/$ – see front matter © 2011 Elsevier B.V. All rights reserved.
doi:10.1016/j.jpowsour.2011.10.107

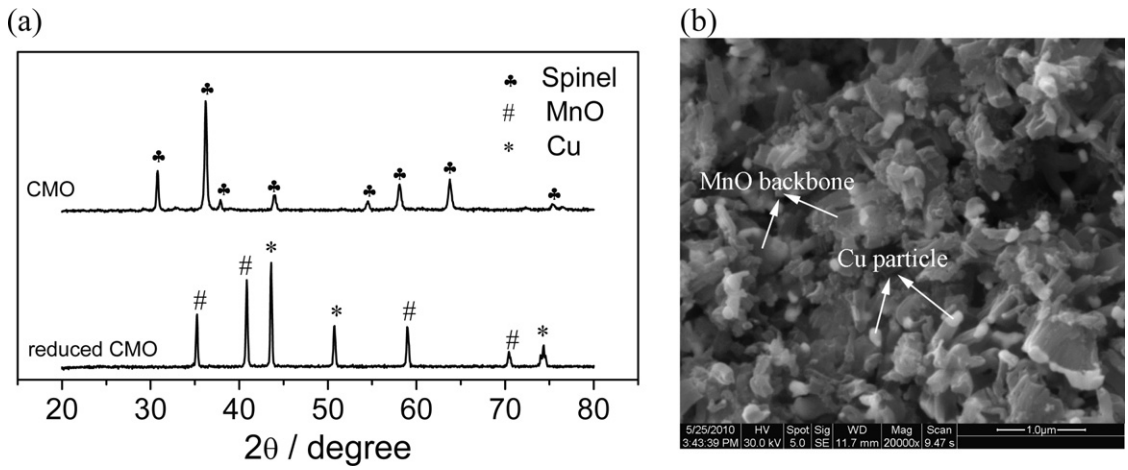

Fig. 1. (a) X-ray diffraction patterns of the pure $Cu_{1.3}Mn_{1.7}O_4$ (CMO) powder (up) and the reduced CMO (down) by CH_4 at 900 °C for 10 h; (b) SEM image of the reduced CMO powder.

2. Experimental

2.1. Materials synthesis and characterization

$Cu_{1.3}Mn_{1.7}O_4$ (CMO) spinel oxide was prepared through a citric acid–nitrate process [11]. Stoichiometric amounts of analytical grade $Cu(NO_3)_2$ (Alfa Aesar, USA) and $Mn(NO_3)_2$ (Alfa Aesar, USA) were dissolved in deionized water, and the concentration of the total metal ions was 0.2 mol L^{-1}. Citric acid was then added to the mixture as chelating and complexing agent, and the mole ratio of the total metal ions:citric acid was controlled around 1:1.5. Ammonium hydroxide (Sigma–Aldrich, NH_3 content 28.0–30.0%) was added to adjust the pH value of the precursor solution to about 6.0. A gel was obtained after the solution was agitated at 70 °C on a hot-plate for 24 h, which was then heat-treated at 400 °C for 5 h in an oven to remove organics and form a precursor powder. The $Cu_{1.3}Mn_{1.7}O_4$ precursor powder was pulverized and then calcined at 950 °C for 8 h. $Sm_{0.2}Ce_{0.8}O_{1.9}$ (SDC) electrolyte material and $La_{0.6}Sr_{0.4}Co_{0.8}Fe_{0.2}O_3$ (LSCF) cathode material were prepared according to a process reported previously [15]. The crystal structure of the powders was examined with X-ray diffraction (XRD) using a Bede D1 X-ray diffractometer (UK, Bede Scientific Ltd.; Cu K_α radiation; operated at 40 kV, 45 mA; $\lambda = 0.15418$ nm), with the diffraction angle ranging from 20° to 80°, a step of 0.02° and a rate of 1.2° min^{-1}.

2.2. Temperature-programmed reduction (TPR)

Before the TPR test, NiO and CMO powders were mixed with SDC powder in a weight ratio of 1:1, respectively. The mixture was then degassed at 400 °C in N_2 followed by a re-oxidation in 10% O_2 at the same temperature. The sample was subsequently cooled down to room temperature and the TPR data was collected in 5% H_2 in Ar with a ramping rate of 10 °C min^{-1} from room temperature to 800 °C.

2.3. Fabrication and electrochemical characterization of single solid oxide fuel cells

NiO (J.T. Baker, USA) and SDC powders with a weight ratio of 1:1 were ball-milled. In addition, 15 wt.% graphite was added as pore former to make sufficient porosity of the anode. NiO–SDC anode substrate and SDC electrolyte were fabricated by a co-pressing method with a stainless-steel mould (15 mm in diameter) under a pressure of about 200 MPa. The anode and electrolyte bilayer was co-sintered at 1400 °C in air for 4 h to obtain a dense SDC electrolyte film (about 70 μm). A slurry consisting of CMO–SDC mixture (in 60:40 weight ratio) and an organic binder (ethyl cellulose and α-terpineol) was then printed on the surface of NiO–SDC anode substrate and fired at 1100 °C for 2 h to produce the anode internal reforming layer. Further, a LSCF–SDC (in 50:50 weight ratio) composite cathode layer and LSCF cathode collector layer were applied onto the electrolyte surface using a brush painting method, followed by firing at 1000 °C for 2 h. The effective cathode area is 0.33 cm^2. A silver grid was printed on the surface of the cathode to collect the cathodic current and silver wire was used as the current lead. Finally, single cells were assembled on alumina tubes using a glass–ceramic bonding/sealing material (Aremco-552 high temperature ceramic adhesive paste).

The prepared cell was measured using the two-electrode method with ambient air as the oxidant and methane (with 3 vol.% water) as the fuel, and the fuel flow rate was 30 ml min^{-1}. After reducing the NiO-containing anode at 600 °C in CH_4 for several hours until a constant open circuit voltage (*OCV*) was obtained, the current–voltage curves and electrochemical impedance spectroscopy (*EIS*) were measured from 600 to 700 °C, and the constant current load test was performed at 650 °C using a VersaStudio electrochemistry analyzer. For *EIS* measurement, the frequency range was from 100 kHz to 0.1 Hz and the AC amplitude was 10 mV. The measured impedance spectra data were fitted and analyzed using the Zview software (Schribner Associates Inc.). After the cell short-term stability test, the microstructure of the cell and the compositions of the selected regions of the cell were characterized by a scanning electron microscopy (SEM) equipped with the energy-dispersive X-ray spectroscopy analysis (EDX) (FEI Quanta 200).

3. Results and discussion

3.1. Characterization of $Cu_{1.3}Mn_{1.7}O_4$ material

Fig. 1(a) shows the XRD patterns of the as-prepared $Cu_{1.3}Mn_{1.7}O_4$ (CMO) powder after calcination in air at 950 °C for 8 h and the reduced CMO powder by methane at 900 °C for 10 h. As it can be seen from this figure, the as-prepared CMO powder exhibits a single spinel phase structure with no detectable impurity phases [11,13]. For the reduced CMO powder, it can be clearly observed that $Cu_{1.3}Mn_{1.7}O_4$ oxide has been reduced into metallic Cu and MnO. This is consistent with that reported in the literature about methane reforming process [13]. Fig. 1(b) shows SEM image of the reduced CMO powder, where a uniformly dispersed

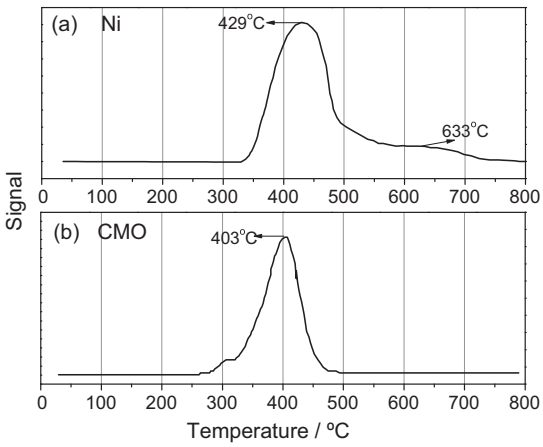

Fig. 2. Temperature-programmed reduction (TPR) profiles of: (a) NiO–SDC and (b); CMO–SDC. The curves were recorded in 5% H_2 balanced in Ar at a ramp rate of 10 °C min^{-1}. The powder was degassed and reoxidized at 400 °C before the TPR test.

fine Cu–MnO particle network has been obtained with the Cu particles having an average size of ~80 nm. The crystallite size of Cu is close to that calculated from the Scherrer equation based on the Cu (1 1 1) diffraction.

3.2. TPR study

Ni plays an important catalytic role in the Ni-based cermet anode for oxidation of H_2 or hydrocarbon fuels. In order to investigate the catalytic activity of Ni and CMO spinel, TPRs of NiO and CMO mixed with SDC samples were carried out, respectively. As it can be seen in Fig. 2(a), there are mainly two reduction peaks for NiO–SDC in the measured temperature range. According to Mori et al. [16], the peak around 429 °C is close to the pure NiO reduction peak and is considered as the bulk NiO free from impact of the SDC support. The peak around 633 °C corresponds to the NiO on the surface of the SDC support, but strong interactions exist between them. As shown in Fig. 2(b), the TPR profile of the CMO–SDC is quite different from that of the NiO–SDC. The peak around 633 °C disappears while an additional shoulder peak appears around 300 °C. The peak at lower temperature was ascribed to the reduction of Cu species in spinel lattice and the higher one was ascribed to the reduction of Mn_2O_3 to MnO via Mn_3O_4, though it is difficult to clearly define their reduction boundary [17]. No peaks were observed in the higher temperature region, suggesting that MnO was highly stable under reducing condition up to 1000 °C. Compared with that of the NiO–SDC shown in Fig. 2(a), the TPR behavior of the CMO–SDC has lower hydrogen consumption, even for the strongest reduction peak, and the location of its maximum shifts from 429 to 403 °C. Such TPR features show significantly different reduction behavior for these two catalyst systems, and the CMO–SDC displays better catalytic activity than that of the Ni–SDC.

3.3. Carbon deposition analysis

Rapid deterioration of the fuel cell performance has been observed with the nickel anode when operating on methane fuel due to the coke formation over the anode surface that limits free gas adsorption and electrochemical oxidation of the fuel [18,19]. It has been widely accepted that carbon forms on the nickel cermet anode in methane fuel mainly by the following two reactions: methane pyrolysis reaction (1) and carbon monoxide disproportionation reaction (Boudouard reaction) (2):

$$CH_4 \rightarrow C + 2H_2 \quad \Delta H^{\ominus}_{298} = 75 \text{ kJ/mol} \tag{1}$$

$$2CO \rightarrow C + CO_2 \quad \Delta H^{\ominus}_{298} = -171 \text{ kJ/mol} \tag{2}$$

where $\Delta H^{\ominus}_{298}$ is the standard enthalpy of the reaction at 298 K. Reaction (1) is favored by increasing temperature, and carbon deposition is mainly caused by the methane pyrolysis reaction when the operating temperature of fuel cell is over 700 °C. Pyrolysis occurs above 700 °C, while the thermodynamic equilibrium of the Boudouard reaction is shifted to the right at lower temperatures, resulting in coke formation [7]. On the other hand, carbon deposition can be suppressed by steam reforming reaction (3) and water gas shift reaction (4) [20]. Steam reforming reaction is favored by elevated temperatures.

$$CH_4 + H_2O \rightarrow CO + 3H_2 \quad \Delta H^{\ominus}_{298} = 206 \text{ kJ/mol} \tag{3}$$

$$CO + H_2O \rightarrow CO_2 + H_2 \quad \Delta H^{\ominus}_{298} = -41 \text{ kJ/mol} \tag{4}$$

In our fuel cell design, SDC is selected as the electrolyte material. Therefore the cell operating temperature can be controlled below 700 °C, which will avoid carbon deposition caused by methane pyrolysis at high temperatures. Further, $Cu_{1.3}Mn_{1.7}O_4$ spinel internal reforming layer fabricated on the NiO–SDC anode surface can effectively convert methane into CO and H_2 before methane flowing into the anode/electrolyte interface. With the increase in CO formed within the cell, carbon deposition can be potentially occurred due to the possible Boudouard reaction. However, because SDC has high oxygen ion conductivity, even if there were some carbon deposited in the electrochemical reaction zone, it could be electrochemically oxidized to CO_2 according to reaction (5) [21]:

$$C + 2O^{2-} \rightarrow CO_2 + 4e^- \tag{5}$$

Fig. 3 shows the SEM image and carbon mapping image of the CMO–SDC internal reforming layer after the cell short–term durability testing in methane. The spots in Fig. 3(b) represent carbon deposition on the surface of the internal reforming layer shown in Fig. 3(a). The increase in the signal indicates the increase in the amount of carbon deposition. It can be seen from Fig. 3(b) that there is very weak signal from the deposited carbon. Therefore, very little carbon deposition has occurred on the surface of the internal reforming layer compared with that on the Ni–ScSZ anode surface modified by GDC ($Gd_{0.2}Ce_{0.8}O_2$) [22], implying that carbon deposition was very limited on the surface of the CMO–SDC internal reforming layer during the cell operation.

SEM image analysis of the cell with internal reforming layer after the electrochemical testing shows that the internal reforming catalyst layer with a thickness of ~30 μm adheres very well to the Ni–SDC anode. Carbon deposition was also investigated by EDX at selected regions of the cell as shown in Fig. 4. The analyses were carried out on the surface of internal reforming layer (region 1, as shown in Fig. 4(a)), within the internal reforming layer close to the Ni–SDC anode layer (region 2, as shown in Fig. 4(b)), and within the Ni–SDC anode layer close to the anode–electrolyte interface (region 3, as shown in Fig. 4(c)), respectively. From the EDX spectra, it can be clearly observed that there are only weak carbon signals detected, either in region 1, region 2, or in region 3. It is well known that the electrochemical reaction active zone of the anode is typically less than 20 μm adjacent to the electrolyte layer at the anode–electrolyte interface [3]. Carbon deposition over this layer would result in reduced active sites for the electrochemical oxidation of the fuel, consequently leading to serious deterioration of the cell performance. The EDX analysis shows that the CMO–SDC internal reforming layer can effectively prevent the anode from carbon deposition, especially in the anode electrochemical reaction zone.

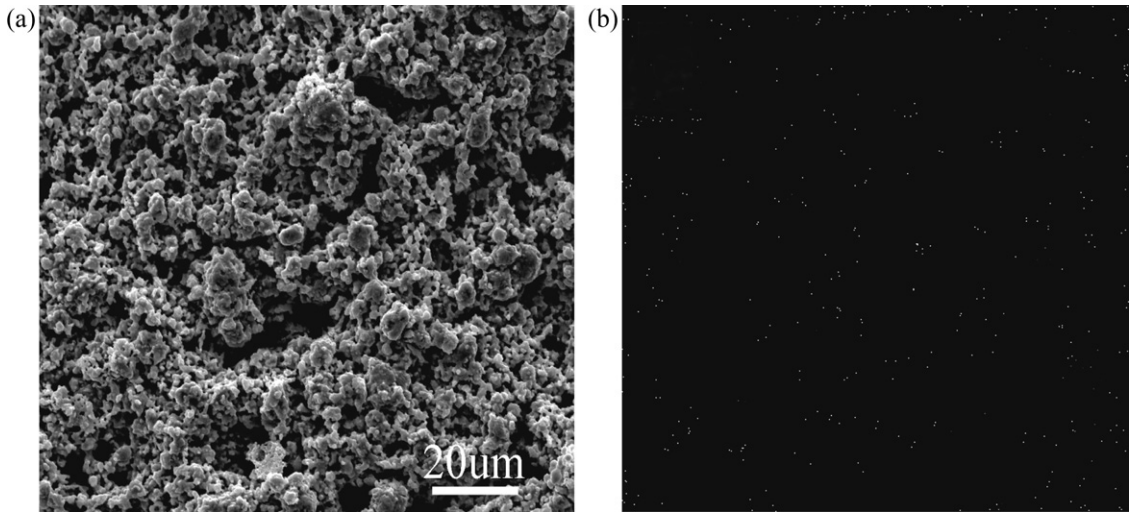

Fig. 3. SEM–EDX photo for CMO–SDC internal reforming layer of the cell after directly operating in methane over 80 h at 650 °C. (a) SEM image of the CMO–SDC free surface; (b) the carbon mapping of the CMO–SDC free surface.

3.4. Cell electrochemical performances

Fig. 5 displays the *I–V* and *I–P* curves of the fuel cell with the CMO–SDC internal reforming layer at different operating temperature. When no internal reforming layer was deposited over the anode, the cell using methane as the fuel produced maximum power densities (*MPDs*) of 113, 179 and 258 mW cm^{-2} at 600, 650 and 700 °C, respectively [11]. The cell output power densities increased to 172, 304 and 375 mW cm^{-2} under the same testing conditions (as shown in Fig. 5) when the CMO–SDC internal reforming layer was applied on the anode. In CuB_2O_4 (B = Fe, Mn, Cr, Ga, Al, etc.) spinel catalysts family, CuMn-based spinel material exhibits the highest selectivity to CO [23]. After the spinel is reduced, well dispersed fine Cu metallic particles with high specific surface area in the MnO matrix will be formed, which can effectively accelerate methane steam reforming to produce H_2 and CO according to reaction (3). The formed H_2 and CO will then diffuse to the anode active layer where they will be electrochemically oxidized to produce H_2O, CO_2 and electrons, as represented in reactions (6) and (7). Since nickel-based cermet anode has higher electrochemical activity for H_2 and CO than methane, the cell operating with methane shows higher power output when the internal reforming layer is applied on the Ni–SDC anode.

$$H_2 + O^{2-} \rightarrow H_2O + 2e^- \quad (6)$$

$$CO + O^{2-} \rightarrow CO_2 + 2e^- \quad (7)$$

Although enhanced cell performance has been obtained upon directly operating in methane fuel with the $Cu_{1.3}Mn_{1.7}O_4$ spinel as the internal reforming layer, it is important to demonstrate that the cells can work stably. Endurance tests have been carried out on a number of cells and stable cell performance has been observed when operating the cells in methane. Fig. 6 shows an example of an SOFC life test for >80 h. The test was carried out in a cell with the internal reforming layer using 30 ml min^{-1} methane fuel under a constant current load of 0.6 A cm^{-2} at 650 °C. In the initial 2 h operation, the cell output increased, probably due to the electrode activation. The cell showed a slight performance drop at around 55 h. This is probably due to the conditioning of the electrode. A stable operation from 55 to 82 h was obtained and the cell was then stopped for microstructural and compositional analysis. Without an internal reforming layer, the conventional Ni–SDC or Ni–GDC anode based SOFCs will typically deactivate quickly and fail <20 h when directly operating in methane fuel [24,25]. For the reduced CuB_2O_4 (B = Fe, Mn, Cr, Ga, Al, etc.) spinel oxide, the stability of metal oxides and the strong interaction between the metal oxides and Cu could lead to an excellent catalyst durability [23]. Although MnO is less active in the reforming reaction, it is relatively stable under reducing condition up to 900 °C and has a strong interaction with Cu particles as shown in Fig. 1. Consequently, inclusion of the $Cu_{1.3}Mn_{1.7}O_4$ internal reforming layer on the Ni–SDC anode has greatly improved the cell performance stability upon direct utilization of methane fuel.

3.5. Cell electrochemical impedance spectra analysis

Fig. 7(a) shows the impedance spectra for the cell running on the methane fuel at different temperature under open circuit condition before the short-term durability test. As the operating temperature increases, the impedance decreases significantly. The measured impedance spectra data were fitted and analyzed using the Zview software. Symbols are the experimental data and lines are the fitted results. The equivalent circuit used for fitting is also provided in Fig. 7(b). Good fitting between the equivalent circuit and the experimental data has been obtained. The impedance spectra are consisted of two arcs, indicating that there are at least two electrode processes corresponding to the fuel cell reaction. A high-frequency inductive component (L) coming from the measuring system is visible at high temperature; the series resistance, R_s, corresponds to the overall ohmic resistance from the electrolyte, electrodes and the lead wires; Q is the constant phase element while (R_1, Q_1) and (R_2, Q_2) correspond to the high and low frequency arcs, respectively. The total interfacial polarization resistance (R_p) of the cell is the sum of R_1 and R_2. Table 1 summarizes the fitted results for the cell reaction at different operating temperatures.

According to the fitted electrode polarization resistances, the activation energy can be calculated and is shown in Fig. 8. The activation energies are 32.9, and 166.3 kJ mol^{-1} for the electrode processes corresponding to the high and low frequency impedance arcs, respectively. The activation energy of the overall electrode polarization resistance is 118.7 kJ mol^{-1}. In the temperature range studied, it is clear that the oxidation reaction in CH_4 is dominated by the low frequency impedance process. In many previous studies concerning H_2 oxidation reaction on Ni–YSZ cermet anodes [26,27], the reaction is generally considered to be limited by two electrode steps, namely, hydrogen dissociative adsorption and diffusion on the Ni surface or hydrogen gas diffusion inside the

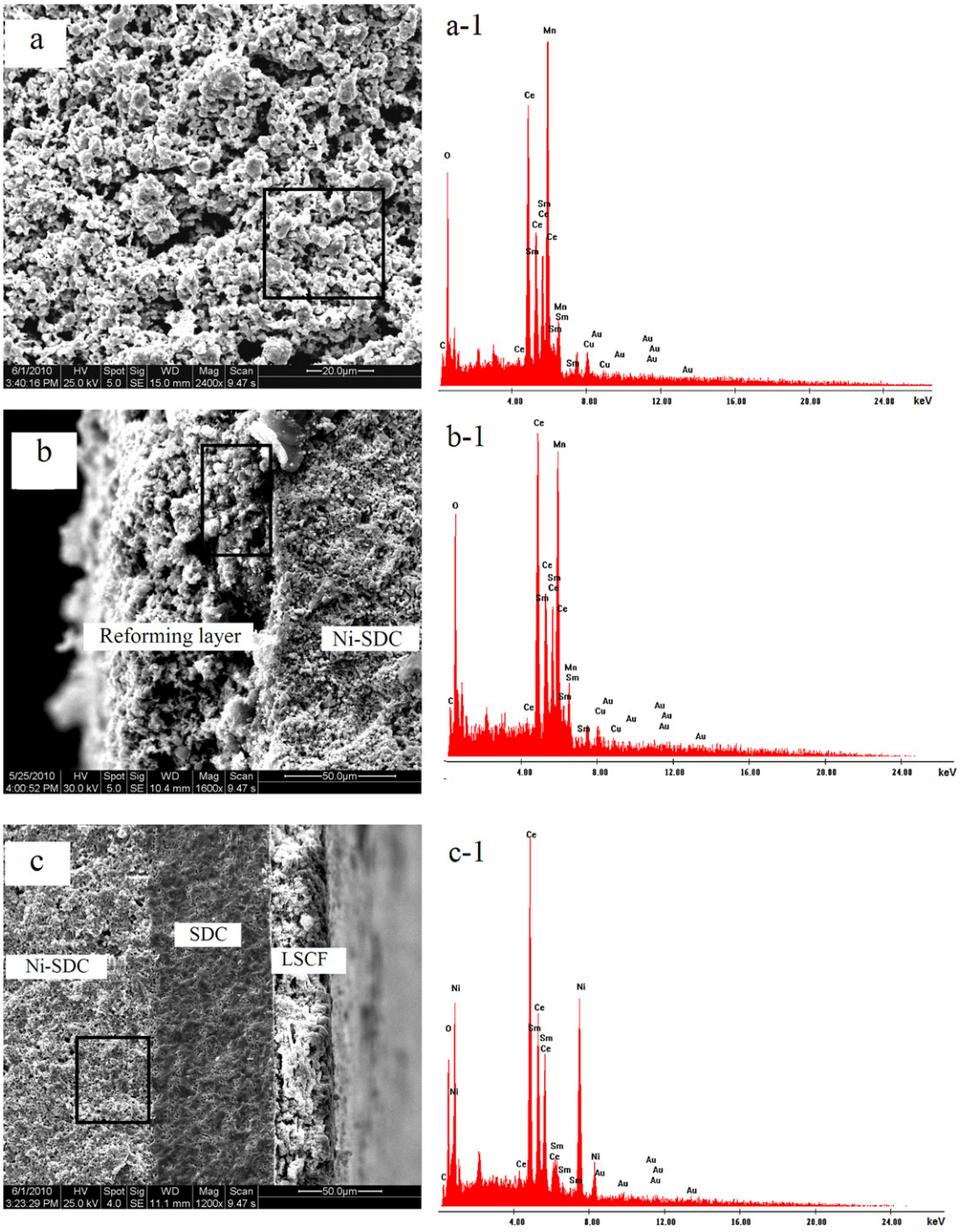

Fig. 4. SEM images and EDX spectra taken from different regions of the cell after operating on methane over 80 h at 650 °C.

porous anode, and the charge transfer reaction at the electrode and electrolyte interface [26]. The electrode process associated with hydrogen dissociative adsorption has much lower activation energy (0–50 kJ mol^{-1}) as compared to the charge transfer process [26,27]. The three phase boundary areas between the Ni electrode, YSZ electrolyte and H_2 reactant gas play a very important role in the reaction kinetics of the H_2 oxidation reaction in the Ni and Ni–YSZ cermet anodes [28]. In our cell design with CH_4 as the

Table 1
Fitting parameters extracted from impedance spectra at different operating temperatures.

	Fitting results						
	L	R_s	R_1	$Q_1/(\Omega\,cm^2\,s^{-n})$	R_2	$Q_2/(\Omega\,cm^2\,s^{-n})$	R_p
600 °C	1.65×10^{-7}	0.395	0.118	0.220	0.522	0.529	0.640
650 °C	2.23×10^{-7}	0.323	0.094	0.200	0.121	0.546	0.215
700 °C	2.04×10^{-7}	0.243	0.074	0.168	0.046	0.619	0.120

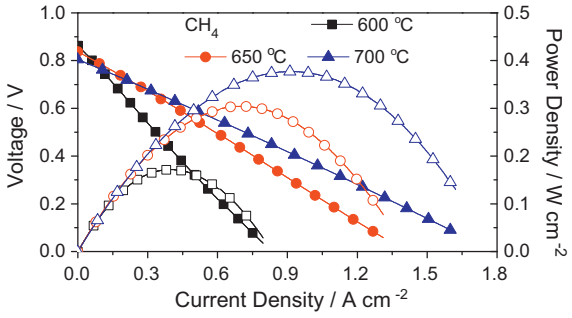

Fig. 5. *I–V* and *I–P* curves of the cell with CMO–SDC internal reforming layer running on wet methane at different operating temperatures.

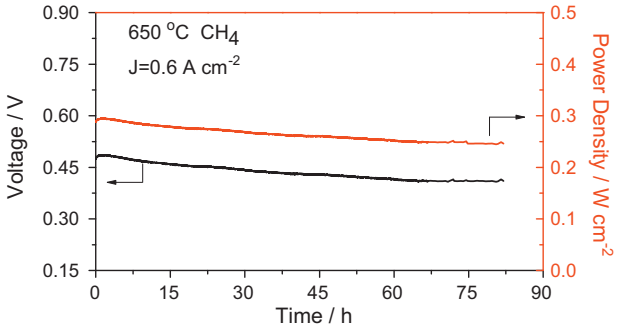

Fig. 6. The cell durability under a constant current of 0.6 A cm^{-2} at 650 °C.

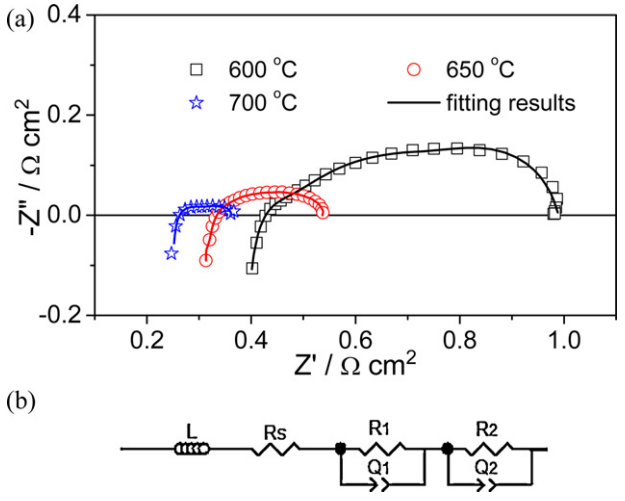

Fig. 7. (a) Impedance spectra of the cell recorded under open circuit voltage at different temperatures; (b) the fitting equivalent circuit.

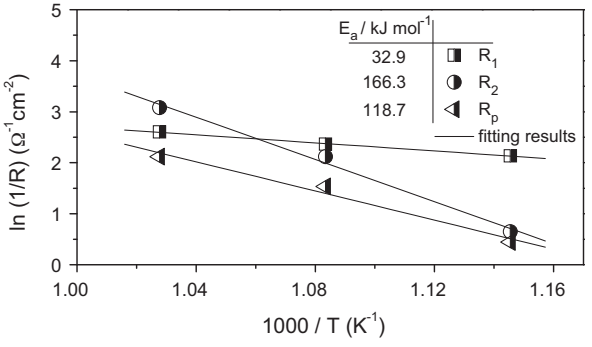

Fig. 8. Arrhenius plots of the fitted electrode polarization resistance according to the fitting equivalent circuit.

fuel, the cell shows similar reaction mechanism to that of the H_2 oxidation reaction on the Ni–YSZ anode, suggesting that active reactants are mainly H_2 or CO in the electrochemical reaction zone. In other words, CMO internal reforming layer has effectively converted methane into CO and H_2 before methane flowing into the anode/electrolyte interface.

4. Conclusions

$Cu_{1.3}Mn_{1.7}O_4$ (CMO) spinel has been synthesized through a citric acid–nitrate process. After reduction by CH_4 at 900 °C for 10 h, well dispersed fine Cu metallic particles in the matrix of MnO have been obtained. TPR result shows that CMO has lower hydrogen consumption and exhibits better catalytic activity than conventional Ni cermet anode. With CMO–SDC as the internal reforming layer, the cell with the configuration of CMO–SDC|Ni–SDC|SDC|LSCF shows enhanced power output of 375 mW cm^{-2} at 700 °C when directly operating with methane as the fuel. Compared with the conventional Ni-based methane-fueled SOFCs, the stability of the cell with CMO–SDC internal reforming layer has been greatly improved. The current work has demonstrated a new cell design to mitigate carbon deposition problem in Ni-based direct methane fueled SOFCs.

Acknowledgements

We gratefully acknowledge the financial support of the South Carolina Space Grant Consortium and Natural Science Foundation of China (NSFC, contract no. 21073129).

References

[1] N.Q. Minh, J. Am. Ceram. Soc. 76 (1993) 563–588.
[2] G.A. Tompsett, C. Finnerty, K. Kendall, T. Alston, N.M. Sammes, J. Power Sources 86 (2000) 376–382.
[3] F. Zhao, A.V. Virkar, J. Power Sources 141 (2005) 79–95.
[4] S.C. Singhal, Solid State Ionics 152–153 (2002) 405–410.
[5] S.P. Jiang, X.J. Chen, S.H. Chan, J.T. Kwok, K.A. Khor, Solid State Ionics 177 (2006) 149–157.
[6] Y.B. Tang, J. Liu, Acta Phys. Chim. Sin. 26 (5) (2010) 1191–1194.
[7] Y.B. Tang, J. Liu, Int. J. Hydrogen Energy 35 (2010) 11188–11193.
[8] R. Peters, E. Riensche, P. Cremer, J. Power Sources 86 (2000) 432–441.
[9] M.M. Liao, W. Wang, R. Ran, Z.P. Shao, J. Power Sources 196 (2011) 6177–6185.
[10] P.K. Cheekatamarla, C.M. Finnerty, J. Cai, Int. J. Hydrogen Energy 33 (2008) 1853–1858.
[11] C. Jin, C.H. Yang, F. Zhao, A. Coffin, F.L. Chen, Electrochem. Commun. 12 (2010) 1450–1452.
[12] E. Lay, G. Gauthier, S. Rosini, C. Savaniu, J.T.S. Irvine, Solid State Ionics 179 (2008) 1562–1566.
[13] K.S. Kang, C.H. Kim, W.C. Cho, K.K. Bae, S.W. Woo, C.S. Park, Int. J. Hydrogen Energy 33 (2008) 4560–4568.
[14] A.L. Pinheiro, A.N. Pinheiro, A. Valentini, et al., Catal. Commun. 11 (2009) 11–14.
[15] C. Jin, J. Liu, W.M. Guo, Y.H. Zhang, J. Power Sources 183 (2008) 506–511.
[16] H. Mori, C.J. Wen, J. Otomo, K. Eguchi, H. Takahashi, Appl. Catal. A 245 (2003) 79–85.
[17] Y. Tanaka, T. Takeguchi, R. Kikuchi, K. Eguchi, Appl. Catal. A 279 (2005) 59–66.
[18] J. Liu, S.A. Barnett, Solid State Ionics 158 (2003) 11–16.
[19] Y.B. Lin, Z.L. Zhan, S.A. Barnett, J. Power Sources 158 (2006) 1313–1316.
[20] K. Ke, A. Gunji, H. Mori, S. Tsuchida, H. Takahashi, K. Ukai, Y. Mizutani, H. Sumi, M. Yokoyama, K. Waki, Solid State Ionics 177 (2006) 541–547.
[21] Y.B. Lin, Z.L. Zhan, J. Liu, S.A. Barnett, Solid State Ionics 176 (2005) 1827–1835.
[22] B. Huang, X.F. Ye, S.R. Wang, H.W. Nie, J. Shi, Q. Hu, J.Q. Qian, X.F. Sun, T.L. Wen, J. Power Sources 162 (2006) 1172–1181.
[23] K. Faungnawakij, N. Shimoda, T. Fukunaga, R. Kikuchi, K. Eguchi, Appl. Catal. A 341 (2008) 139–145.
[24] H. Lv, D.J. Yang, X.M. Pan, J.S. Zheng, C.M. Zhang, W. Zhou, J.X. Ma, K. Hu, Mater. Res. Bull. 44 (2009) 1244–1248.
[25] W. Wang, W. Zhou, R. Ran, R. Cai, Z.P. Shao, Electrochem. Commun. 11 (2009) 194–197.
[26] S.P. Jiang, S.P.S. Badwal, Solid State Ionics 123 (1999) 209–224.
[27] S.P. Jiang, W. Wang, Y.D. Zhen, J. Power Sources 147 (2005) 1–7.
[28] A. Bieberle, L.P. Meier, L.J. Gauckler, J. Electrochem. Soc. 148 (2001) A646–A656.